

Beyond the Rigid Lid: Baroclinic Modes in a Structured Atmosphere

JACOB P. EDMAN AND DAVID M. ROMPS

Department of Earth and Planetary Science, University of California, Berkeley, and Climate and Ecosystem Sciences Division, Lawrence Berkeley National Laboratory, Berkeley, California

(Manuscript received 1 May 2017, in final form 13 August 2017)

ABSTRACT

The baroclinic-mode decomposition is a fixture of the tropical-dynamics literature because of its simplicity and apparent usefulness in understanding a wide range of atmospheric phenomena. However, its derivation relies on the assumption that the tropopause is a rigid lid that artificially restricts the vertical propagation of wave energy. This causes tropospheric buoyancy anomalies of a single vertical mode to remain coherent for all time in the absence of dissipation. Here, the authors derive the Green's functions for these baroclinic modes in a two-dimensional troposphere (or, equivalently, a three-dimensional troposphere with one translational symmetry) that is overlain by a stratosphere. These Green's functions quantify the propagation and spreading of gravity waves generated by a horizontally localized heating, and they can be used to reconstruct the evolution of any tropospheric heating. For a first-baroclinic two-dimensional right-moving or left-moving gravity wave with a characteristic width of 100 km, its initial horizontal shape becomes unrecognizable after 4 h, at which point its initial amplitude has also been reduced by a factor of $1/\pi$. After this time, the gravity wave assumes a universal shape that widens linearly in time. For gravity waves on a periodic domain the length of Earth's circumference, it takes only 10 days for the gravity waves to spread their buoyancy throughout the entire domain.

1. Introduction

Much of the atmospheric tropical-dynamics literature has relied on spectrally discretized and truncated models that reduce the primitive equations to a set of shallow-water equations for the first one or two baroclinic modes (e.g., Matsuno 1966; Gill 1980; Neelin and Held 1987; Mapes 1993). This class of simple models is capable of replicating important aspects of the tropical atmospheric circulation. For example, some studies (e.g., Wheeler and Kiladis 1999; Hendon and Wheeler 2008) have documented features in the tropical spectra of outgoing longwave radiation that appear quite similar to the linear equatorial waves predicted by Matsuno (1966). Others (e.g., Gill 1980; Neelin and Held 1987) have constructed simple models that capture many of the observed features of steady tropical circulations using only the first baroclinic mode.

The spectral discretization used by these simple models is only formally justified if the tropopause behaves like a rigid lid, and the spectral truncation to the first one or two modes is valid only if the heating has a

particularly simple structure. It has indeed been observed that the first one or two baroclinic modes dominate diabatic heating profiles in the tropical troposphere, at least around mesoscale convective systems (Mapes and Houze 1995). Past work often interprets first- and second-baroclinic-mode heating as corresponding to deep convective and stratiform clouds, respectively (e.g., Mapes 2000; Haertel and Kiladis 2004). However, the tropopause is far from being a rigid lid, and in a semi-infinite atmosphere, any heat source confined to the troposphere excites waves with a continuous spectrum of vertical structures, even if the heating is dominated by a single baroclinic mode (Pandya et al. 1993; Mapes 1998; Lindzen 2003).

A further objection to this spectral discretization and truncation comes from considering the response to transient heating in a model with a rigid lid. Bretherton and Smolarkiewicz (1989) introduced the canonical description of gravity wave adjustment in a nonrotating fluid, in which wave fronts of compensating subsidence propagate away from the heat source at discrete gravity wave speeds corresponding to each baroclinic mode. This model has proved useful for understanding how convective clouds may initiate convection in their local

Corresponding author: Jacob P. Edman, jedman@berkeley.edu

environments (Mapes 1993) and for parameterizing the interaction of convection and large-scale circulations (e.g., Raymond and Zeng 2000; Cohen and Craig 2004; Edman and Romps 2014). However, this picture of purely horizontal wave radiation is at best incomplete: it predicts that wave fronts produced by a pulse of heating will propagate forever unless there is some dissipation in the system. To prevent this pathological behavior, simple models based on one or two baroclinic modes often invoke strong damping in the form of Rayleigh friction and Newtonian cooling, with time scales of about 1–10 days (e.g., Matsuno 1966; Chang 1977; Gill 1980; Wu et al. 2000; Sobel et al. 2001; Sugiyama 2009; Chan and Shepherd 2014). Some have found this need for strong damping unsettling (e.g., Battisti et al. 1999), but recent work has suggested that it could be produced by convective momentum transport (Lin et al. 2008; Romps 2014).

As other studies have pointed out (e.g., Pandya et al. 1993), the upward radiation of wave energy modifies the rigid-lid picture, smoothing out sharp wave fronts that would otherwise propagate forever in the absence of any dissipative friction or radiation. This diffusion of sharp wave fronts occurs because the vertical component of the group velocity for hydrostatic gravity waves is proportional to the horizontal wavenumber. Therefore, the

largest horizontal wavenumbers are the first to radiate out of the troposphere (Gill 1982), rapidly smoothing out any sharp features in the tropospheric gravity wave. Eventually, all of the nonzero horizontal wavenumbers radiate into the stratosphere, leaving the troposphere with a nonpropagating, horizontally uniform buoyancy anomaly.

Some studies have suggested that internal gravity waves radiate out of the troposphere on time scales relevant to dynamics. Mapes (1998) attempted to parameterize the smoothing of wave fronts emanating from a mesoscale convective system using a Gaussian kernel. And, Yano and Emanuel (1991) found that upward radiation of wave energy suppresses the growth of the wind-induced surface heat exchange (WISHE) instability for all but the longest equatorial modes.

In another study, Chumakova et al. (2013, hereafter CRT) found a set of exponentially decaying solutions to the linearized two-dimensional Boussinesq equations in a layer of fluid with constant buoyancy frequency N_1 (i.e., the troposphere) overlain by a layer of fluid with a buoyancy frequency N_2 greater than N_1 (i.e., the stratosphere). We will refer to these exponentially decaying solutions as CRT modes. A single CRT mode of buoyancy [from Eqs. (17) and (18) of CRT] can be written as¹

$$b_{k,m}^{\text{CRT}}(x, z, t) = \begin{cases} b_0 \sin(mz) \exp\left(-i\frac{N_1|k|}{m}t + ikx\right) & \text{for } z \leq H \\ b_0 \frac{N_2^2}{N_1^2} \sin(mH) \exp\left[-i\frac{N_1|k|}{m}t + ikx - i\frac{N_2}{N_1}m(z-H)\right] & \text{for } z > H \end{cases}, \quad (1)$$

where

$$m = \frac{n\pi + i \tanh^{-1}(N_1/N_2)}{H} \quad (2)$$

is a complex vertical wavenumber, n is an integer, k is a horizontal wavenumber, H is the height of the tropopause, and b_0 is a constant with dimensions of buoyancy. This buoyancy distribution can be generated at time $t = 0$ in an initially quiescent atmosphere by applying a heating of $Q = b_{k,m}^{\text{CRT}}(x, z, 0)\delta(t)$, where δ is the Dirac delta function. The resulting pattern of buoyancy

propagates horizontally with speed $\text{Re}(N_1/m)$ and decays exponentially with an e -folding time of $-1/\text{Im}(N_1|k|/m)$.

In principle, the CRT modes can be used to construct solutions to some initial-value problems, but there are a host of problems with this approach: the CRT modes do not have the same vertical structure as rigid-lid normal modes; the CRT modes are not orthogonal; the CRT modes are divergent in the $N_2 = N_1$ limit; the buoyancy in the initial state of each CRT mode is not confined to the troposphere; and the energy density of each CRT mode grows exponentially without bound as you move upward in the stratosphere. The unboundedness is essential to how the CRT modes work: the CRT modes are constructed to decay exponentially in time, but to have an upward-propagating pattern of gravity waves in the stratosphere that decays exponentially with time, the pattern must grow exponentially with height.

¹ There are a couple of typos in Eq. (18) of CRT. The expressions for ρ_n and p_n are missing factors of $i\rho_0$ and $i\rho_0 N_1^2$, respectively. In Eq. (4), we have also extended the CRT modes into the stratosphere by enforcing continuity of $(1/N^2)\partial_z b$ and $(1/N^2)\partial_z \partial_t b$ at $z = H$, which guarantee continuity of u and w .

Another way in which the CRT modes are unphysical is that they fail to generate a steady state in response to a steady tropospheric heating. In a two-dimensional (2D) Boussinesq fluid at rest, the response to a steady heating

is steady and finite within an ever-expanding region centered at the location of the heating. To see that the CRT modes do not achieve this state, first consider the heating

$$Q(x, z, t) = \begin{cases} B_0 \sin(mz)\delta(x)\delta(t) & \text{for } z \leq H \\ B_0 \frac{N_2^2}{N_1^2} \sin(mH) \exp\left[-i\frac{N_2}{N_1}m(z-H)\right] \delta(x)\delta(t) & \text{for } z > H \end{cases}, \quad (3)$$

where m is defined as in Eq. (2) with integer n . Here and throughout, we will use a lowercase b to denote a buoyancy (m s^{-2}), an uppercase B to denote a horizontally integrated buoyancy ($\text{m}^2 \text{s}^{-2}$), and Q to denote a

heating or, in other words, a tendency of buoyancy (m s^{-3}). Since the Fourier transform of $\delta(x)$ is $1/\sqrt{2\pi}$, this buoyancy evolves as

$$b_m^{\text{CRT}}(x, z, t) = \frac{B_0}{2\pi b_0} \int_{-\infty}^{\infty} dk b_{k,m}^{\text{CRT}}(x, z, t) = \begin{cases} \frac{B_0}{2\pi} \text{Im} \left[\sin(mz) \left(\frac{1}{N_1 t/m + x} + \frac{1}{N_1 t/m - x} \right) \right] & \text{for } z \leq H \\ \frac{B_0}{2\pi} \frac{N_2^2}{N_1^2} \text{Im} \left\{ \sin(mH) \exp[-i(N_2/N_1)m(z-H)] \right. \\ \left. \times \left(\frac{1}{N_1 t/m + x} + \frac{1}{N_1 t/m - x} \right) \right\} & \text{for } z > H \end{cases}. \quad (4)$$

This solution has a left-moving pulse of buoyancy and a right-moving pulse of buoyancy that both smear out with time. As with the single- k solution in Eq. (1), this has an energy density that grows exponentially with height in the stratosphere. This behavior was baked in by the heating in Eq. (3), which had to be chosen that way in order to make use of the CRT modes. When integrated horizontally and temporally, that heating grows exponentially with height in the stratosphere.

From this solution, we can find the solution to a heating that has the same spatial structure as Eq. (3) but has a Heaviside unit step function of time $\mathcal{H}(t)$ instead of a $\delta(t)$ (i.e., the heating is switched on at $t = 0$ and held on). The solution to this is $\int_0^t dt' b_m^{\text{CRT}}(x, z, t') \mathcal{H}(t)$, which is proportional to $\log[1 - (N_1 t/mx)^2]$, which grows logarithmically without bound. Since this behavior occurs for any m satisfying Eq. (2), the CRT modes do not admit any steady-state solutions to a steady heating.

The left panel of Fig. 1 illustrates this pathology for an $n = 1$ heating (closely approximating a first-baroclinic structure in the troposphere) of the form in Eq. (3) with $\delta(t)$ replaced with $\mathcal{H}(t)$. The values of H , N_1 , and N_2 are chosen to be representative of the tropical atmosphere. Based on Fig. 2, which shows the mean of 3-hourly soundings from the Department of Energy’s Atmospheric Radiation Measurement (ARM) site in Darwin,

Australia, from 18 January to 3 February 2006, these values are set to $H = 17 \text{ km}$, $N_1 = 0.01 \text{ s}^{-1}$ and $N_2 = 0.025 \text{ s}^{-1}$ here and throughout the paper. For ease of reference, these values are printed in Table 1. In the left panel of Fig. 1, each colored line plots the time series of midtropospheric buoyancy at a specific distance from the origin. For example, the darkest blue curve is the buoyancy at $x = 10 \text{ km}$, which will feel the leading edge of the gravity wave pass over it at a normalized time of $\text{Re}(N_1/m)t = 10 \text{ km}$. The darkest red curve is the buoyancy at $x = 100 \text{ km}$, which will feel the leading edge of the gravity wave pass over it at a normalized time of $\text{Re}(N_1/m)t = 100 \text{ km}$. If these solutions behaved as expected from rigid-lid thinking, then the buoyancy at each of these locations would plateau at a value of $2\text{Re}(N_1/m)/B_0$ shortly after the wave front has passed. Instead, the buoyancy at all of these locations continues to rise logarithmically. This undesirable behavior is a consequence of the stratospheric heating that is baked into the CRT modes. As we will see in section 2d, steady heating that is confined to the troposphere generates a steady buoyancy field.

In this study, we take a different approach than CRT. Rather than seek a set of vertical modes for an atmosphere without a rigid lid at the tropopause, we solve the initial-value problem directly. In section 2, we derive a

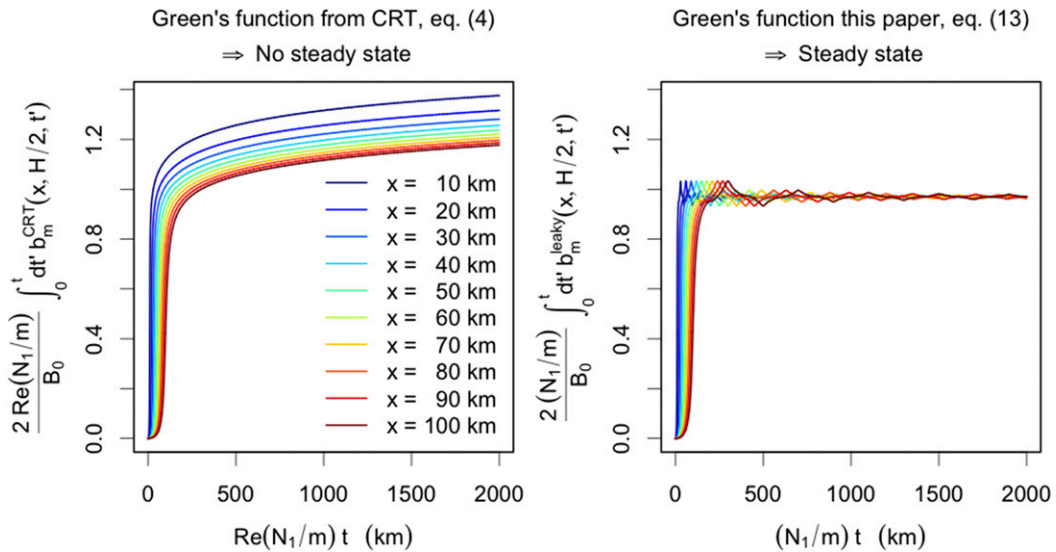


FIG. 1. (left) The time series of midtropospheric buoyancy for a variety of distances from the origin, ranging from 10 to 100 km, for a steady $n = 1$ heating (approximating a first baroclinic mode in the troposphere) that is held on for all $t > 0$, which is obtained by integrating the CRT Green's function in Eq. (4). The time on the abscissa is normalized by the propagation speed of the wave front, $\text{Re}(N_1/m)$. The buoyancies on the ordinate are normalized by $2\text{Re}(N_1/m)/B_0$, which is simply the value to which the midtropospheric buoyancy would asymptotically approach shortly after the wave front passes. (right) As in (left), but for the Green's function presented in Eq. (13).

Green's function for a pulse of buoyancy in the troposphere with baroclinic vertical structure for the simplest atmosphere without a rigid lid at the tropopause: the two-dimensional, nonrotating Boussinesq equations with two layers of constant but differing stratification. In the subsequent sections, we explore how this simple change to a more realistic upper boundary condition results in buoyancy anomalies that quickly spread out as they propagate, in stark contrast to the rigid-lid case.

$$N = \begin{cases} N_1 & \text{for } 0 \leq z \leq H \\ N_2 & \text{for } H < z \end{cases}, \quad (6)$$

where H is the tropopause. When $N_2 > N_1$, this is a simple analog for Earth's atmosphere in which the troposphere is capped by the more stratified stratosphere. The derivation in section 2d, however, applies equally well to any value of N_2/N_1 from zero to infinity.

2. The leaky-lid Green's function

The Boussinesq equations describing hydrostatic linear perturbations to a two-dimensional, nonrotating, stratified fluid at rest are

$$\partial_t u = -\frac{\partial_x p}{\rho_0}, \quad (5a)$$

$$0 = -\frac{\partial_z p}{\rho_0} + b, \quad (5b)$$

$$\partial_t b = -N^2 w + Q, \quad (5c)$$

$$0 = \partial_x u + \partial_z w, \quad (5d)$$

where u is the horizontal speed, w is the vertical speed, ρ_0 is a constant density, p is the pressure perturbation, b is the buoyancy, and Q is the buoyancy source or, in other words, the heating. Let N be piecewise constant in height such that

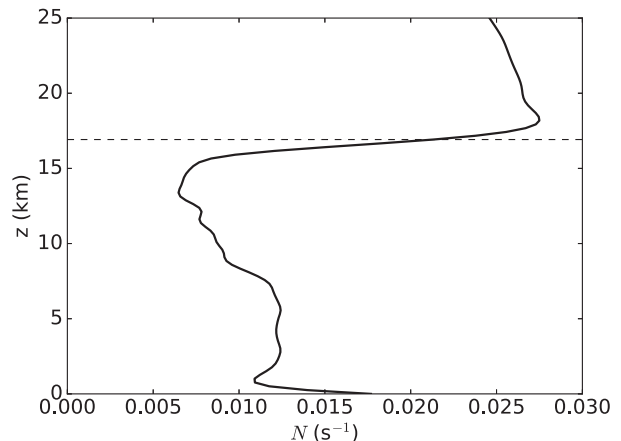


FIG. 2. Mean profile of the Brunt-Väisälä frequency N calculated from soundings taken every 3 h at the Darwin ARM site from 18 Jan to 3 Feb 2006. The dashed line denotes the cold-point tropopause at 16.9 km.

TABLE 1. Default parameter values, which are typical for Earth's tropics, used throughout the paper unless otherwise specified.

| Parameter | Symbol | Value |
|---------------------------------------|-----------|-----------------------|
| Buoyancy frequency in the troposphere | N_1 | 0.01 s^{-1} |
| Depth of the troposphere | H | 17 km |
| Stratification ratio | N_2/N_1 | 2.5 |

In the following subsections, we will review the Green's functions for a troposphere with a rigid lid ($N_2 = \infty$) and a troposphere with no lid ($N_2 = N_1$) and then present the Green's function for a troposphere with a leaky lid ($N_1 < N_2 < \infty$), which, as we will see, connects the rigid-lid and no-lid limits. To derive any of these Green's functions, we write the set of Boussinesq equations [Eqs. (5)] as a wave equation for b ,

$$\partial_t^2 \partial_z^2 b + N^2 \partial_x^2 b = \partial_t \partial_z^2 Q, \quad (7)$$

and we seek a solution for a baroclinic tropospheric heating of the form

$$Q(x, z, t) = B_0 \sin(mz) \mathcal{H}(H - z) \delta(x) \delta(t), \quad (8)$$

where B_0 is a constant, H is the depth of troposphere, and m is taken to be one of the baroclinic modes (i.e., $m = n\pi/H$, where n is an integer).

a. Green's function for a rigid lid

To begin, we reproduce the well-known solution for an atmosphere with a rigid lid at the tropopause, which corresponds to $N_2 = \infty$. The rigid lid requires $w = 0$ at $z = H$, so we can formally decompose the solutions to Eq. (7) into a set of vertical normal modes with discrete eigenvalues. This decomposition gives the traditional baroclinic modes, or rigid-lid modes, which are sines (for b and w) and cosines (for p and u) with nodal or antinodal points at the surface and tropopause (Gill 1982). Each baroclinic mode is governed by a set of shallow-water equations with wave speed N_1/m , where m is the eigenvalue corresponding to a particular baroclinic mode.

For a troposphere with a rigid lid, the Green's function—that is, the solution to Eq. (7) for a baroclinic pulse specified by Eq. (8)—is

$$b_m^{\text{rigid}}(x, z, t) = \frac{B_0}{2} [\delta(N_1 t/m + x) + \delta(N_1 t/m - x)] \times \mathcal{H}(t) \sin(mz) \mathcal{H}(H - z). \quad (9)$$

This describes two delta-function pulses of buoyancy propagating to the left and right with the same baroclinic vertical structure as the forcing. The nature of this

solution follows directly from the discrete spectrum of vertical modes for a layer of fluid with a rigid lid. By design, the source specified by Eq. (8) excites exactly one of the normal modes of this system, which travels with a constant horizontal wave speed $c = N_1/m$. In the absence of dissipation, these pulses will propagate forever.

b. Green's function for no lid

Next, consider a troposphere with no lid, which corresponds to $N_2 = N_1$. In this case, the Green's function—that is, the solution to Eq. (7) for a baroclinic pulse specified by Eq. (8)—was found by Pandya et al. (1993) to be

$$b_m^{\text{no_lid}}(x, z, t) = \frac{B_0}{2\pi} \cos(mH) \sin(HN_1 t/x) \sin(N_1 t z/x) \times \left(\frac{1}{N_1 t/m + x} + \frac{1}{N_1 t/m - x} \right). \quad (10)$$

Despite the appearance of singularities at $x = \pm N_1 t/m$, the solution is smooth there; at those locations, the divergence from the $1/(N_1 t/m \pm x)$ terms is canceled by the $\sin(HN_1 t/x)$ term since m is an integer multiple of π/H . The two pulses of buoyancy propagate horizontally at the same speed as in the rigid-lid case, but they spread out into smooth blobs rather than retaining their delta-function shape.

Another notable difference from the rigid-lid solution is the complex vertical structure of the buoyancy field. Unlike the rigid-lid solution, which has the same vertical structure as the heating, the no-lid buoyancy field projects onto every baroclinic mode: the buoyancy is not all of the same baroclinicity as the heating. This reflects the fact that the baroclinic modes are not the vertical eigenfunctions of the system when the rigid lid is raised beyond the tropopause. In fact, when there is no lid at all, as in this case, the eigenvalue spectrum becomes continuous. The relationship between the continuous and discrete spectra is precisely that of the continuous and discrete Fourier transforms. As the spatial domain increases in size, the discrete transform approaches the continuous one. Despite this, the linearized governing Eqs. (5) require that the horizontally integrated buoyancy maintains the same baroclinic structure as the source for all time, regardless of N_2 . For example, in the case of a first-baroclinic source, the horizontally integrated buoyancy is first baroclinic for all time. This property can most easily be seen by integrating Eq. (5c) over x and noting that the integral of w over x must be zero by continuity. Remarkably, it can be confirmed numerically that the horizontal integral of $b_m^{\text{no_lid}}$ equals $B_0 \sin(mz) \mathcal{H}(H - z)$.

To get a quantitative sense of how the no-lid solution compares to the rigid-lid solution, consider the buoyancy at $x = \pm N_1 t/m$, which are the centers of the propagating pulses. Taking the limit of Eq. (10) as $|x| \rightarrow N_1 t/m$, we find

$$b_m^{\text{no-lid}}(\pm N_1 t/m, z, t) = \frac{B_0 m^2 H}{2\pi N_1 t} \sin(mz). \quad (11)$$

Note that all of the buoyancy at $x = \pm N_1 t/m$ is contained in the same vertical mode m as the initial perturbation. Note, also, that the amplitude goes as $1/t$. Since the horizontally integrated buoyancy is constant and projects only onto the baroclinic mode of the source, this implies that the width of the left-moving or right-moving pulse is proportional to t ; more specifically, its width is approximately $\pi N_1 t/m^2 H$.

In summary, the one-way-propagating buoyancy pulses can be described as propagating at a constant speed of $c = N_1/m$ at their center and with edges that spread away from its center at a speed of $\pi N_1/2m^2 H = (\pi/2mH)c$. We will see in section 2d how this is modified for $N_2 > N_1$.

c. Simple model for the decay of amplitude

What causes the pulses of buoyancy to decay in amplitude and spread out? It is illuminating to think of the counterpropagating pulses of buoyancy as packets of internal gravity waves propagating away from the source. Without a rigid lid at the tropopause, internal gravity waves can propagate out of the troposphere. The vertical group velocity for internal gravity waves is proportional to the horizontal wavenumber, which means that shorter waves radiate out of the troposphere faster than longer waves. It is this process that causes the dispersal of the initial delta functions noted above. After a sufficiently long time, all that remains is a nonpropagating, horizontally uniform buoyancy anomaly in the troposphere. Note that the net heating to the troposphere is the same whether or not there is a rigid lid at the tropopause: wave energy can propagate upward, but the buoyancy is still confined to the troposphere.

We can construct a simple model for the decay in amplitude at $|x| = N_1 t/m$ by considering the upward radiation of gravity waves. From the dispersion relation for hydrostatic gravity waves defined by Eq. (7), we find that $\omega = N_1 |k|/m$, where k is the horizontal wavenumber, so the horizontal speed of a hydrostatic gravity wave is $c_x = N_1/m$, and the vertical group velocity of a hydrostatic gravity wave is $c_{gz} = N_1 |k|/m^2$. A natural time scale τ_k for a gravity wave of horizontal wavenumber k to radiate up and out of the troposphere

is the depth of the troposphere H divided by the vertical group velocity, or

$$\tau_k = \frac{m^2 H}{N_1 |k|}. \quad (12)$$

Therefore, we posit that the amplitude of a plane wave of buoyancy in the troposphere decays like $\exp(-t/\tau_k)$.

For a buoyancy pulse that begins as a delta function in x , we can approximate the evolution of the resulting counterpropagating buoyancy pulses (or wave packets) by modifying the rigid-lid solution in Eq. (9) to include this exponential decay of gravity waves. Taking the Fourier transform of Eq. (9) yields

$$\begin{aligned} \tilde{b}_m^{\text{rigid}}(k, z, t) &= \frac{1}{\sqrt{2\pi}} \int_{-\infty}^{\infty} dx e^{ikx} b_m^{\text{rigid}}(x, z, t) \\ &= \frac{B_0}{2\sqrt{2\pi}} (e^{ikN_1 t/m} + e^{-ikN_1 t/m}) \sin(mz). \end{aligned}$$

We can approximate the decay of gravity waves that occurs in the no-lid atmosphere by multiplying this Fourier-transformed rigid-lid solution by $\exp(-t/\tau_k)$, that is,

$$\tilde{b}_m^{\text{no-lid}}(k, z, t) \approx \frac{B_0}{2\sqrt{2\pi}} (e^{ikN_1 t/m} + e^{-ikN_1 t/m}) e^{-t/\tau_k} \sin(mz).$$

Since $1/\tau_k$ is proportional to $|k|$, this modification does not alter the horizontally integrated buoyancy, which is contained in the $k = 0$ mode. By performing an inverse Fourier transform evaluated at $|x| = N_1 t/m$, we get

$$\begin{aligned} b_m^{\text{no-lid}}(\pm N_1 t/m, z, t) &\approx \frac{1}{\sqrt{2\pi}} \int_{-\infty}^{\infty} dk e^{\pm ikN_1 t/m} \tilde{b}_m^{\text{no-lid}}(k, z, t) \\ &= \frac{1 + 2m^2 H^2}{1 + 4m^2 H^2} \frac{B_0 m^2 H}{\pi N_1 t} \sin(mz) \\ &\approx \frac{B_0 m^2 H}{2\pi N_1 t} \sin(mz), \end{aligned}$$

which is the expression previously derived in Eq. (11). This confirms Eq. (12) as the approximate residence time scale for plane waves in the troposphere.

d. Green's function for a leaky lid

Having explored the limiting cases of a rigid lid and no lid, we can turn to our goal of deriving the Green's function for the case of a troposphere with a leaky lid, which corresponds to $N_1 < N_2 < \infty$. For details of the derivation, see the appendix. The Green's function—that is, the solution to Eq. (7) for a baroclinic pulse specified by Eq. (8)—is found to be

$$b_m^{\text{leaky}}(x, z, t) = \begin{cases} \frac{B_0}{2\pi} \frac{N_1}{N_2} + \left(\frac{N_2}{N_1} - \frac{N_1}{N_2} \right) \sin^2(HN_1 t/x) \times \left(\frac{1}{N_1 t/m + x} + \frac{1}{N_1 t/m - x} \right) \times \sin(N_1 t z/x) & \text{for } z \leq H \\ \frac{B_0}{2\pi} \frac{N_1}{N_2} + \left(\frac{N_2}{N_1} - \frac{N_1}{N_2} \right) \sin^2(HN_1 t/x) \times \left(\frac{1}{N_1 t/m + x} + \frac{1}{N_1 t/m - x} \right) \frac{N_2}{2N_1} \\ \times \left\{ \left(\frac{N_2}{N_1} + 1 \right) \sin \left[\frac{N_1 t z}{x} + \left(\frac{N_2}{N_1} - 1 \right) \frac{N_1 t (z - H)}{x} \right] \right. & \text{for } z > H \\ \left. + \left(\frac{N_2}{N_1} - 1 \right) \sin \left[\frac{N_1 t H}{x} + \frac{N_2 t (H - z)}{x} \right] \right\} \end{cases} \quad (13)$$

This solution is valid over the full range of N_2/N_1 , from 0 to ∞ , which means that it encompasses both the rigid-lid and no-lid solutions. When $N_2/N_1 = 1$, b_m^{leaky} equals $b_m^{\text{no-lid}}$; that is, it gives the solution for constant N from Eq. (10). In the limit of $N_2/N_1 \rightarrow \infty$, $b_m^{\text{leaky}} = b_m^{\text{rigid}}$; that is, it gives the solution for a rigid-lid tropopause from Eq. (9).

Figure 3 compares the no-lid solution ($N_1 = N_2 = 0.01 \text{ s}^{-1}$) and the leaky-lid solution ($N_1 = 0.01 \text{ s}^{-1}$ and $N_2 = 0.025 \text{ s}^{-1}$) at $t = 1 \text{ h}$ in response to the tropospheric heating in Eq. (8) with $H = 17 \text{ km}$, $m = \pi/H$, and $B_0 = 1 \text{ m}^2 \text{ s}^{-2}$. Compared to the no-lid solution, the first-baroclinic gravity waves are more coherent in the troposphere (i.e., they are more compact in the horizontal and have higher peak buoyancies). At the tropopause, there is a discontinuity in buoyancy at the tropopause due to the discontinuity of N^2 in Eq. (5c). In the stratosphere, the oscillations in buoyancy have a vertical wavelength that is shorter by the factor of N_1/N_2 , and their amplitude is greater. As with the no-lid solution, it can be confirmed that the leaky-lid solution has the following properties: b_m^{leaky} satisfies Eq. (7) with $Q = 0$ for all $t > 0$; $(1/N^2)\partial_t b_m^{\text{leaky}}$ and $(1/N^2)\partial_z \partial_t b_m^{\text{leaky}}$ are continuous across the tropopause, guaranteeing continuity of u and w there; the horizontal integral of b_m^{leaky} equals $B_0 \sin(mz) \mathcal{H}(H - z)$; and b_m^{leaky} is zero for all $|x| > 0$ at $t = 0$.

Although t appears in several places in Eq. (13), the temporal evolution of b_m^{leaky} is surprisingly simple. Defining $\hat{x} = mx/N_1 t$, we can write b_m^{leaky} as

$$b_m^{\text{leaky}}(x, z, t) = \frac{B_0 m}{2\pi N_1 t} \frac{N_1}{N_2} + \left(\frac{N_2}{N_1} - \frac{N_1}{N_2} \right) \sin^2(mH/\hat{x}) \times \left(\frac{1}{1 + \hat{x}} + \frac{1}{1 - \hat{x}} \right) \quad \text{for } z \leq H. \quad (14)$$

Writing b_m^{leaky} in this way makes clear that the shape of the buoyancy distribution is invariant in time: the buoyancy distribution simply stretches out linearly in time (i.e., position \hat{x} in the distribution travels away from the origin at speed $\hat{x}N_1/m$) as its overall amplitude decreases as $1/t$. Therefore, one plot of b_m^{leaky} is sufficient to illustrate its evolution for all time.

Plots of b_m^{leaky} are shown in the top row of Fig. 4 for cases of, from left to right, no lid and first baroclinic ($N_2/N_1 = 1$ and $m = \pi/H$); no lid and second baroclinic ($N_2/N_1 = 1$ and $m = 2\pi/H$); leaky lid and first baroclinic ($N_2/N_1 = 2.5$ and $m = \pi/H$); and leaky lid and second baroclinic ($N_2/N_1 = 2.5$ and $m = 2\pi/H$). For an apples-to-apples comparison, these are plotted on the same color scale at a time in their evolution when the pulses have reached a common distance from the origin (i.e., at a time for the second-baroclinic pulses that is twice the time for the first-baroclinic pulses). The abscissa ranges over plus and minus twice that distance. The ordinate ranges over the full depth of the troposphere.

At the center of each pulse, b_m^{leaky} evaluates to

$$b_m^{\text{leaky}}(\pm N_1 t/m, z, t) = \frac{N_2}{N_1} \frac{B_0 H m^2}{2\pi N_1 t} \sin(mz) \quad \text{for } z \leq H. \quad (15)$$

Since the buoyancy pulses travel at a speed of $c_{gx} = N_1/m$, their amplitude is proportional to $m/c_{gx}t$. For the same distance traveled (i.e., for the same value of $c_{gx}t$), the amplitude of the wave is proportional to the baroclinicity (i.e., proportional to m). Since the width of the buoyancy pulse is inversely proportional to the amplitude, this means that when a second-baroclinic pulse has traveled 100 km, it is twice as compact in the horizontal as the second-baroclinic pulse when it reaches 100 km. In summary, the n th-baroclinic pulse

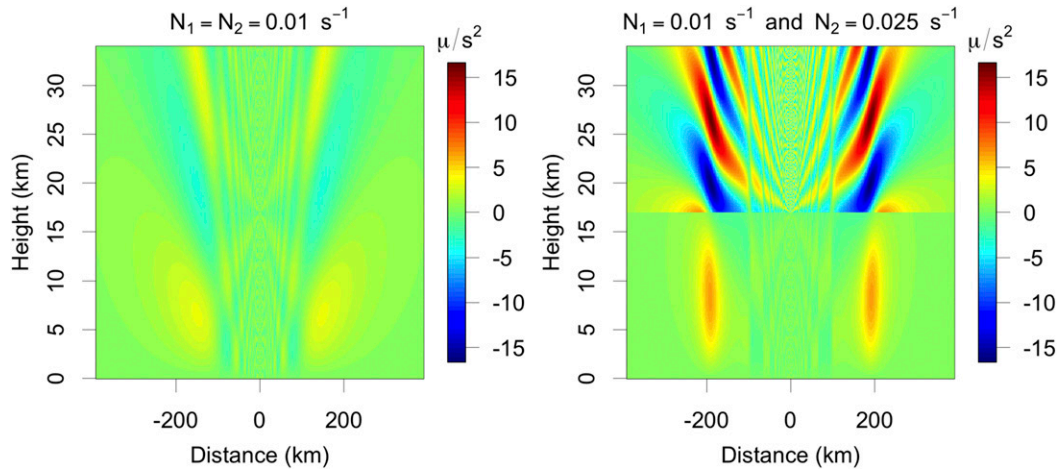


FIG. 3. (left) The no-lid solution $b_m^{\text{no-lid}}$ at $t = 1$ h in an atmosphere with $N_1 = N_2 = 0.01 \text{ s}^{-1}$ that was subjected to the heating given by Eq. (8) with $H = 17$ km, $m = \pi/H$, and $B_0 = 1 \text{ m}^2 \text{ s}^{-2}$. (right) As in (left), but for b_m^{leaky} with $N_1 = 0.01 \text{ s}^{-1}$ and $N_2 = 0.025 \text{ s}^{-1}$.

spreads out at $1/n^2$ the rate per time, and $1/n$ the rate per distance, as compared to a first-baroclinic pulse.

Although the buoyancy pulse at $x = \pm N_1 t/m$ has the same baroclinicity as the initial heating, this is not generally true at other x . This is expected since any initial vertical structure that is zero in the stratosphere is not a normal mode of the leaky-lid atmosphere. The eigenvalue spectrum is continuous for any atmosphere that is unbounded in the z direction, so any such initial vertical structure projects onto an infinite number of normal modes, all of which have different phase speeds. These different components of the initial buoyancy distribution radiate away from the initial heat source at different

speeds and thus begin decohering immediately, leading to the complicated horizontal and vertical structure of $b_m^{\text{no-lid}}$ for $t > 0$, which is visible in the top row of Fig. 4. Mathematically, this complexity stems from the tz/x argument in Eq. (13).

Given this complexity, how can we make contact with the standard rigid-lid paradigm? Is there some way that we can write b_m^{leaky} in terms of the rigid-lid modes even though the rigid-lid modes are not normal modes of the leaky-lid atmosphere? The answer is yes: we could simply write b_m^{leaky} as a sum of rigid-lid modes. But this approach is of little conceptual advantage if, say, a first-baroclinic heating generates a

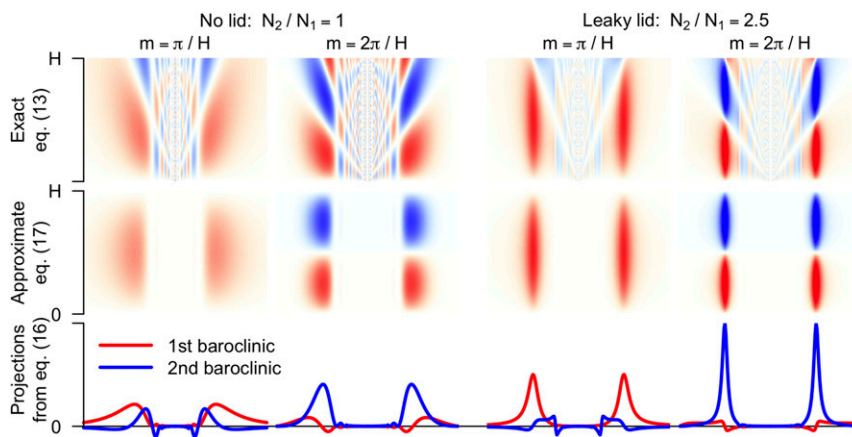


FIG. 4. (top) The Green's function b_m^{leaky} in Eq. (13) for all combinations of $N_2/N_1 \in (0, 1)$ and $m \in (\pi/H, 2\pi/H)$ on a common color scale at the times when the pulses have reached a common distance, with red being positive and blue being negative. (middle) As in (top), but for the approximation of b_m^{leaky} given in Eq. (17). (bottom) The projections of b_m^{leaky} onto the first-baroclinic and second-baroclinic rigid-lid modes, as given by Eq. (16).

buoyancy pulse that projects strongly onto higher-baroclinic modes.

We can quantify these contributions by projecting b_m^{leaky} onto the various baroclinic modes. The projection of b_m^{leaky} onto baroclinic mode m' , which we will denote by $a_{m,m'}^{\text{leaky}}$, is

$$\begin{aligned} a_{m,m'}^{\text{leaky}}(x,t) &= \frac{2}{H} \int_0^H dz \sin(m'z) b_m^{\text{leaky}}(x,z,t) \\ &= \frac{2B_0 N_1 t x^2}{\pi m m' H} \frac{\sin^2(HN_1 t/x)}{\frac{N_1}{N_2} + \left(\frac{N_2}{N_1} - \frac{N_1}{N_2}\right) \sin^2(HN_1 t/x)} \\ &\quad \times \frac{\cos(mH)\cos(m'H)}{[(N_1 t/m)^2 - x^2][(N_1 t/m')^2 - x^2]}. \end{aligned} \quad (16)$$

For the four cases shown in the top row of Fig. 4, the projections onto the first and second baroclinic modes are shown in the bottom row of Fig. 4. These are

$$\begin{aligned} b_m^{\text{leaky}}(x,z,t) &\approx \frac{B_0}{2\pi} \frac{\sin^2(HN_1 t/x)}{\frac{N_1}{N_2} + \left(\frac{N_2}{N_1} - \frac{N_1}{N_2}\right) \sin^2(HN_1 t/x)} \\ &\quad \times \frac{x}{mH} \left[-\frac{1}{(N_1 t/m + x)^2} + \frac{1}{(N_1 t/m - x)^2} \right] \sin(mz) \quad \text{for } z \leq H. \end{aligned} \quad (17)$$

This approximation has the great advantage of having a rigid-lid vertical structure—that is, the $\sin(mz)$ —while still retaining the horizontal decoherence generated by the leaky lid.

This approximation to b_m^{leaky} is plotted in the middle row of Fig. 4. For the no-lid atmosphere, the approximation misses much of the structure of the buoyancy, especially for a first-baroclinic heating. For a leaky-lid atmosphere, however, the approximation is quite accurate.

Finally, let us return to Fig. 1. The right panel shows the response to a first-baroclinic heating that is confined to the troposphere and is turned on at time $t = 0$. Unlike the CRT modes, which must be excited by heating the stratosphere as well, the atmosphere reaches a steady state in response to this steady tropospheric heating. Since any steady tropospheric heating can be constructed out of the b_m^{leaky} Green's functions, this tells us that, for a leaky-lid atmosphere, any steady heating confined to the troposphere will generate a steady response.

e. Leaky-lid wave decay

The preceding analysis tells us about the evolution of buoyancy caused by a heating confined to $x = 0$ in the

plotted on common axes with the red curves representing the projection onto the first baroclinic mode and the blue curves representing the projection onto the second baroclinic mode. In the no-lid troposphere, a first-baroclinic heating generates a buoyancy pattern that projects strongly onto the second baroclinic mode; as seen in the bottom-left panel of Fig. 4, the maximum amplitude of the $m' = 2\pi/H$ projection is nearly as large as the maximum amplitude of the $m' = \pi/H$ projection. For the leaky lid with a realistic N_2/N_1 , however, a first-baroclinic heating generates a buoyancy pattern that projects predominantly onto the first baroclinic mode.

Based on these findings, we conclude that, unlike in a no-lid atmosphere, the projection of the buoyancy onto its original vertical structure is a good approximation in a leaky-lid atmosphere with a realistic stratification jump. This means, for example, that we can approximate b_m^{leaky} by $a_{m,m}^{\text{leaky}} \sin(mz)$:

troposphere. But what about a heating that is sinusoidal in x ? How does the leaky lid modify the tropospheric residence time for such waves?

In principle, we could use the Green's function b_m^{leaky} to calculate the evolution of a horizontally sinusoidal heating, but in practice, we were unable to find a way to perform this calculation analytically. Instead, we can make an educated guess based on what we have learned so far and then check that guess against a numerical calculation. In Eq. (11), we introduced a time scale for waves in the no-lid troposphere, and a comparison of Eqs. (11) and (15) suggests a simple modification for the leaky-lid troposphere. Equations (11) and (15) are the amplitudes of the tropospheric buoyancy at $x = \pm N_1 t/m$ for the no-lid and leaky-lid cases, respectively. These expressions differ only by an overall factor of N_2/N_1 . Since amplitude and width of a buoyancy pulse are inversely related, this means that a one-way-propagating buoyancy pulse widens N_1/N_2 times slower in the presence of a leaky lid. Since the emission of waves from the troposphere is responsible for widening the pulse, this implies that waves exit the troposphere N_1/N_2 times slower in the leaky-lid case compared to the no-lid case and, therefore, reside in

the troposphere N_2/N_1 times longer. Therefore, Eq. (12) generalizes to

$$\tau_k = \frac{N_2}{N_1} \frac{m^2 H}{N_1 |k|}. \quad (18)$$

This time scale exhibits the behavior we expect from studying the Green's function. Namely, the residence time is longer for longer waves (smaller $|k|$) and for more rigid lids (larger N_2/N_1).

f. Numerical validation of the wave time scale

To confirm that the time scale in Eq. (18) is a good approximation for a freely propagating gravity wave in an atmosphere with two layers of differing N , we performed a series of numerical simulations using Dedalus, a flexible, open-source, Python-based framework for solving partial differential equations (www.dedalus-project.org). Dedalus is a spectral solver, and we decompose the domain using a Chebyshev basis in the z direction and Fourier modes in the horizontal. We solve the linearized Boussinesq system (5a)–(5d) on a periodic domain of width $L = 3000$ km, with rigid boundaries at the top and bottom of the domain. The tropopause is located at $H = 17$ km, and the rigid top is placed at 170 km, which is sufficiently high to prevent reflected waves from reentering the troposphere for the duration of the simulation.

To test Eq. (18), we initialize the system with a buoyancy perturbation confined to the troposphere, characterized by a single horizontal wavenumber k and vertical structure corresponding to a single baroclinic mode m . While we are ultimately interested in the amplitude of the buoyancy anomaly, diagnosing the wave energy, which is proportional to the amplitude squared, provides a straightforward (and single signed) way of bookkeeping in this simple simulation setup. We compare the evolution of the wave energy in the troposphere to the time scale predicted by Eq. (18), bearing in mind that, because energy is proportional to amplitude squared, the decay time scale for energy is $\tau_k/2$. Each simulation is run for at least τ_k , over which we expect the energy in the troposphere to undergo two e -foldings. We run a total of 80 simulations, corresponding to all combinations of $m = \pi/H$ and $m = 2\pi/H$; $N_2/N_1 = 1, 2, 3, 4$, and 5 ; and $k = 2\pi n/L$ for integer values of n from 3 through 10, which correspond to horizontal wavelengths ranging from 300 to 1000 km. At each time step, the buoyancy is projected onto the baroclinic mode of the original heating and the tropospheric energy in that mode is calculated. The decay time scale is then estimated as -2 times the inverse of the slope of the linear

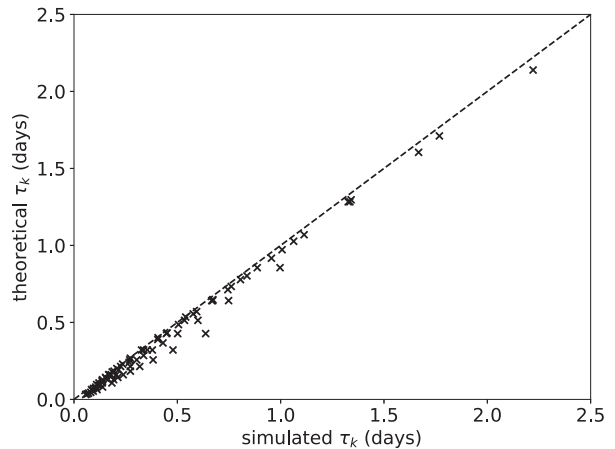


FIG. 5. Simulated tropospheric decay time scale τ_k vs that predicted from Eq. (18) for 80 simulations, which encompass all combinations of $N_2/N_1 = 1, 2, 3, 4$, and 5 , and $k = 2\pi n/3000 \text{ km}^{-1}$ for integer values of n from 3 through 10, for both the first and second vertical mode ($m = \pi/H, 2\pi/H$).

regression of the logarithm of tropospheric energy versus time. In Fig. 5 τ_k calculated from each simulation is plotted against the theoretical τ_k from Eq. (18), along with a dashed one-to-one line. Figure 5 shows very good agreement between the theory and simulation for most parameter values, confirming that the approximate time scale in Eq. (18) correctly characterizes the emission rate of internal gravity waves from an Earthlike troposphere.

3. Lifetime of a pulse of buoyancy

We are now prepared to investigate how a heating of finite width propagates through a two-dimensional troposphere. In principle, we can use the Green's function to calculate how any buoyancy distribution evolves to a horizontally uniform final state. For simplicity, we focus here on heatings that have a top-hat distribution in the horizontal,

$$Q = b_0 \mathcal{H}(a/2 - |x|) \delta(t) \sin(mz), \quad (19)$$

where a is the width of the heating. This generates a buoyancy distribution at $t = 0^+$ that is given by $b_m^{\text{top,hat}}(x, z, 0^+) = b_0 \mathcal{H}(a/2 - |x|) \sin(mz)$.

To find out how this buoyancy evolves in time, we can convolve this initial buoyancy distribution with the Green's function [i.e., with the b_m^{leaky} from Eq. (13)]. Before we do that, however, let us see if we can learn something about its behavior by considering the residence time scales for its Fourier components. The Fourier transform of $b_m^{\text{top,hat}}(x, z, 0^+)$ is

$$\begin{aligned}\tilde{b}_m^{\text{top_hat}}(k, z, 0^+) &= \frac{1}{\sqrt{2\pi}} \int_{-\infty}^{\infty} dx e^{ikx} b_m^{\text{top_hat}}(x, z, 0^+) \\ &= \frac{2b_0}{\sqrt{2\pi}} \frac{\sin(ak/2)}{k} \sin(mz) \mathcal{H}(H-z).\end{aligned}\quad (20)$$

The Fourier transform of the same amount of horizontally integrated buoyancy concentrated at $x=0$ [i.e., $b_m^{\text{leaky}}(x, z, 0^+)$ from Eq. (13) with $B_0 = ab_0$] is

$$\begin{aligned}\tilde{b}_m^{\text{leaky}}(k, z, 0^+) &= \frac{1}{\sqrt{2\pi}} \int_{-\infty}^{\infty} dx e^{ikx} b_m^{\text{leaky}}(x, z, 0^+) \\ &= \frac{ab_0}{\sqrt{2\pi}} \sin(mz) \mathcal{H}(H-z).\end{aligned}\quad (21)$$

Taylor expanding Eq. (20) in k , we find

$$\tilde{b}_m^{\text{top_hat}}(k, z, 0^+) = \tilde{b}_m^{\text{leaky}}(k, z, 0^+) \left(1 - \frac{a^2 k^2}{24} + \dots \right).$$

For $|k|$ satisfying $a^2 k^2/24 \ll 1$ (i.e., for $|k| \lesssim 1/a \ll 2\sqrt{6}/a$), the Fourier transform of $\tilde{b}_m^{\text{top_hat}}$ is practically indistinguishable from the Fourier transform of $\tilde{b}_m^{\text{leaky}}$.

Since waves emanate from the troposphere on a time scale proportional to their wavenumber, there will be a time τ^{melt} when wavenumbers $|k| > 1/a$ will have mostly left the troposphere. After that time, $\tilde{b}_m^{\text{top_hat}}(k, z, t)$ is practically indistinguishable from $\tilde{b}_m^{\text{leaky}}(k, z, t)$. We refer to τ^{melt} as the time scale for ‘‘melting’’ because this is the time by which the initial horizontal shape of the buoyancy pulse has melted away. Based on the preceding argument, we can define τ^{melt} as the time at which wavenumber $1/a$ has experienced an e -folding of decay; that is, we define τ^{melt} as the τ_k from Eq. (18) with $k = 1/a$,

$$\tau^{\text{melt}} = \frac{N_2}{N_1} \frac{m^2 Ha}{N_1}. \quad (22)$$

By Eq. (15), the amplitude of b_m^{leaky} at $x = \pm N_1 \tau^{\text{melt}}/m$ and $t = \tau^{\text{melt}}$ is $b_0/2\pi$.

We can now summarize the evolution of the initial top-hat pulse. At time $t = am/2N_1$, the top-hat buoyancy pulse of magnitude b_0 and width a splits into two pulses, each with magnitude $b_0/2$ and width a , one of which is right moving and the other left moving. At time $t = \tau^{\text{melt}}$, each of the unidirectional pulses has melted down to a peak amplitude of $b_0/2\pi$ and is indistinguishable from an initial delta-function buoyancy pulse. For $t > \tau^{\text{melt}}$, the buoyancy evolves as b_m^{leaky} with the amplitude at $x = \pm N_1 t/m$ equal to $b_0 \tau^{\text{melt}}/2\pi t$.

Figure 6 compares the evolution of the initial top hat (solid red), as calculated numerically by convolution with the Green’s function, against the evolution of an initial delta-function source (dashed green) with the same horizontally integrated buoyancy for the case of $N_2/N_1 = 2.5$. Also shown is the evolution of the top-hat pulse for a rigid lid (dashed black; i.e., for $N_2/N_1 = \infty$). The abscissa is a normalized distance in which unity is the distance traveled in an amount of time equal to τ^{melt} . As expected, the top-hat pulse has become indistinguishable from an initial delta-function pulse by the time $t = \tau^{\text{melt}}$.

We can perform a further check of τ^{melt} by numerically convolving an initial top-hat distribution with the Green’s function b_m^{leaky} from Eq. (13) and diagnosing the time when the amplitude at $|x| = N_1 t/m$ equals $b_0/2\pi$. The top panel of Fig. 7 shows the amplitude of the right-moving half of a first-baroclinic top hat at $x = N_1 t/m$ for $N_2/N_1 = 1, 2.5, 5$, and 10. The x axis is normalized by τ^{melt} so that the curves are independent of the width of the initial top hat. The first-baroclinic Green’s function amplitude [i.e., $b_m^{\text{leaky}}(N_1 t/m, H/2, t)$] is given by the dashed black line. As the right mover and left mover separate at small t/τ^{melt} , there are undulations in the buoyancy distribution that cause the buoyancy to briefly exceed its initial value of $b_0/2$. By $t/\tau^{\text{melt}} = 1$, though, all the curves have converged to the Green’s function amplitude.

The bottom panel of Fig. 7 shows the approximate τ^{melt} from Eq. (22) plotted against the τ^{melt} diagnosed from the time it takes for the numerically integrated, right-moving, first-baroclinic, top-hat pulses to decrease their peak amplitude to $b_0/2\pi$. The top hats are integrated for all combinations of $a = 100, 500, 2000, 4000$, and 8000 km, and $N_2/N_1 = 1, 2.5, 5$, and 10. These points all fall very close to the black dashed one-to-one line.

A few things are notable about the lifetimes of buoyancy anomalies implied by τ^{melt} . First, the time scale is proportional to N_2/N_1 so that as $N_2/N_1 \rightarrow \infty$, $\tau^{\text{melt}} \rightarrow \infty$ too, which is what we expect for the rigid-lid limit. It is also proportional to the width of the pulse, so wider buoyancy anomalies retain their horizontal shape longer. Finally, it is quadratic in m , the baroclinic mode of the initial anomaly. This has potentially significant implications for the wave spectrum of equatorial Kelvin waves: the second-baroclinic pulses retain their original shapes 4 times as long as first-baroclinic pulses.

In general, these decay time scales are quite fast. For a first-baroclinic buoyancy pulse ($m = \pi/H$) in an Earth-like atmosphere ($N_2/N_1 = 2.5$, $N_1 = 0.01 \text{ s}^{-1}$, and $H = 17 \text{ km}$) with a width of 100 km, the original horizontal shape of the left-moving and right-moving buoyancy pulses melts away in only 4 h, which is how long it takes

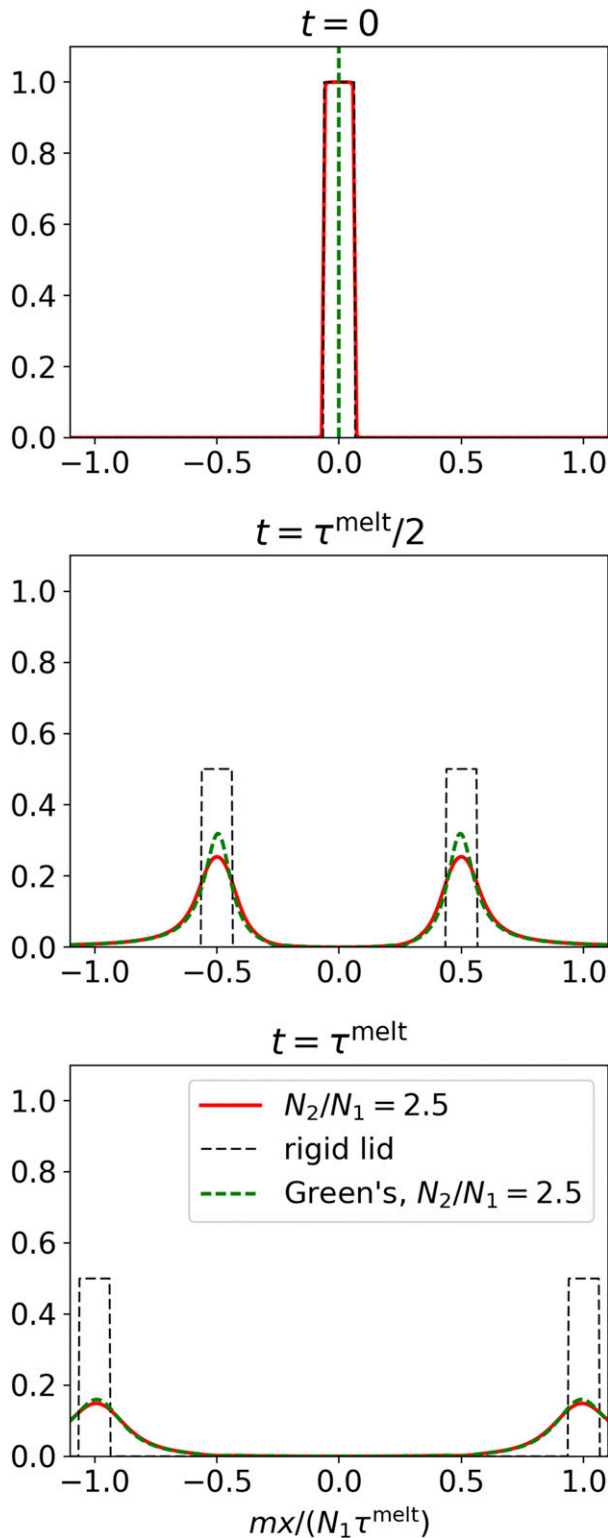


FIG. 6. The red solid line shows the projection of buoyancy from a first-baroclinic top-hat heating onto the first baroclinic mode at (top) $t = 0$, (middle) $\tau^{\text{melt}}/2$, and (bottom) τ^{melt} for $N_2/N_1 = 2.5$, which is found by numerically convolving a top hat with the baroclinic Green's function in Eq. (13). The green dashed line shows the baroclinic Green's function in Eq. (13) with the same profile of horizontally integrated buoyancy. This is an excellent approximation to the top hat for times greater than τ^{melt} in Eq. (22). The abscissa is the distance normalized by the baroclinic wave speed (N_1/m) times τ^{melt} .

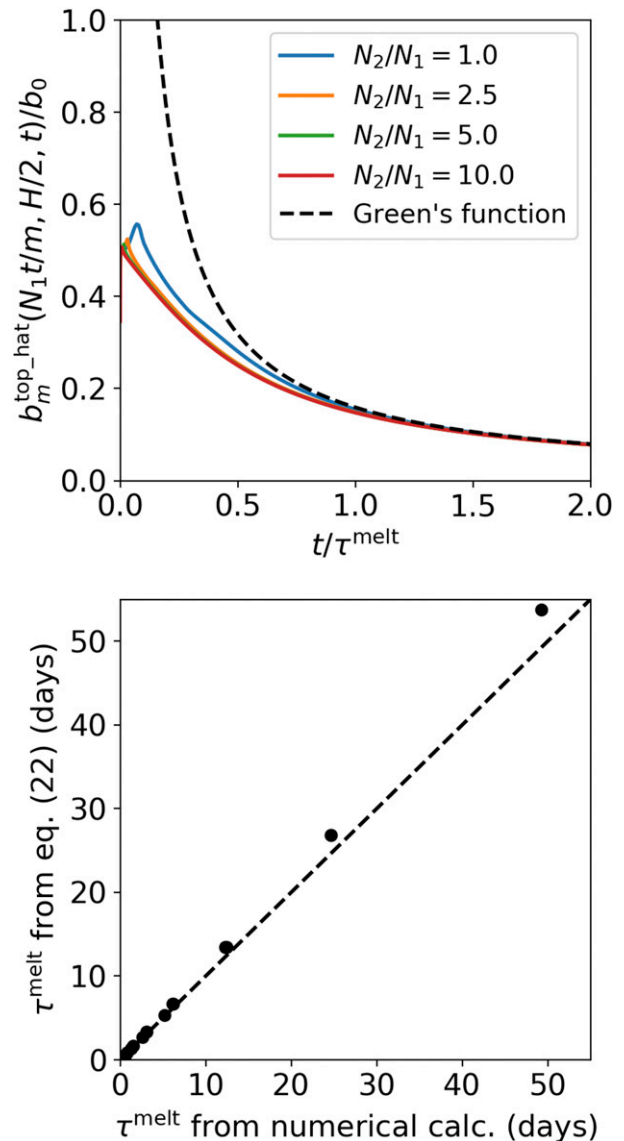


FIG. 7. (top) Fraction of the initial peak buoyancy at $x = N_1 t/m$ as a function of t/τ^{melt} for the right-moving half of a first-baroclinic top-hat pulse of buoyancy, for $N_2/N_1 = 1, 2.5, 5,$ and 10 . (bottom) Estimated τ^{melt} from Eq. (22) plotted against the actual τ^{melt} for first-baroclinic top hats with $a = 100, 500, 2000, 4000,$ and 8000 km, for $N_2/N_1 = 1, 2.5, 5,$ and 10 . The actual τ^{melt} is found by numerically integrating the Green's function in Eq. (13) and finding the time when the buoyancy at $x = N_1 t/m$ drops below $b_0/2\pi$.

each pulse to travel about 800 km from their origin. By that time, each of the pulses has been reduced in amplitude by a factor of $1/\pi$. After this time, the amplitudes decrease as $1/t$ so that, by 8 h, the peak amplitudes have been reduced by another factor of 2.

Although the melting time depends on the characteristic width of the initial pulse of heating, the time to homogenize that heating over a periodic domain is

independent of the initial pulse width. To homogenize over a periodic domain of length L , we must wait a time equal to τ_k from Eq. (18) with $k = 2\pi/L$. For a first-baroclinic pulse on a periodic domain of length L equal to Earth's equatorial circumference of 40 000 km, this homogenization takes about 10 days. This is a remarkably short period of time: an isolated pulse of tropospheric heating generates left-moving and right-moving pulses that reduce to horizontal wavenumbers 1 and 2 by day 2.5, to horizontal wavenumber 1 by day 5, and to an approximately uniform heating around the entire 40 000-km-long domain by day 10.

4. Conclusions

Assuming that the tropical tropopause is a rigid lid greatly simplifies tropical wave dynamics but is not physically justifiable and leads to a choice between the spurious persistence of buoyancy anomalies in the troposphere or using unrealistically strong damping. In this study, we show that replacing the rigid lid with an overlying layer of stratified fluid resolves this difficulty. We have derived Eq. (13), which is the Green's function for a two-dimensional, nonrotating, Boussinesq fluid composed of two layers of constant but differing buoyancy frequencies, which are meant to represent the troposphere and stratosphere. This solution is valid for any ratio of the buoyancy frequencies in the two layers. It includes the rigid-lid solution (an infinitely stratified upper layer) and the no-lid solution (a stratosphere with the same stratification as the troposphere) as limiting cases. We have used this Green's function to show that the dispersive nature of upward internal gravity wave propagation damps away buoyancy anomalies in Earth's troposphere on time scales from hours to days, which are comparable to the linear-damping time scales used in simple models of the tropical atmosphere. This naturally leads to the speculation that simple models of the atmosphere with rigid lids at the tropopause may require strong Rayleigh friction or Newtonian cooling in part because they lack this process.

Of course, the dispersion of vertically propagating internal gravity waves is not equivalent to a linear damping (e.g., Rayleigh friction or Newtonian cooling). While both processes smooth out buoyancy anomalies, linear damping also removes the horizontal mean buoyancy anomaly. On the other hand, vertically propagating gravity waves leave behind a steady, horizontally uniform buoyancy anomaly, and in a steady state, this must be removed by a domain-mean diabatic cooling.

Acknowledgments. This work was supported primarily by the U.S. Department of Energy's Atmospheric

System Research, an Office of Science, Office of Biological and Environmental Research program; Lawrence Berkeley National Laboratory is operated for the DOE by the University of California under Contract DE-AC02-05CH11231. JPE acknowledges support from the National Science Foundation Graduate Research Fellowship under Grant 1106400. The authors also thank Brian Mapes, David Raymond, and an anonymous reviewer for their helpful comments.

APPENDIX

Deriving the Green's function

The path to our solution for an atmosphere with different N in the troposphere and stratosphere adheres closely to the derivations published by Lin and Smith (1986) and Pandya et al. (1993) for an atmosphere with constant N .

We begin by rewriting the two-dimensional, linearized Boussinesq equations [Eqs. (5)] as wave equations for w in each layer:

$$\partial_t^2 \partial_z^2 w_1(x, z, t) + N_1^2 \partial_x^2 w_1(x, z, t) = \partial_x^2 Q, \quad 0 \leq z \leq H, \quad (\text{A1a})$$

$$\partial_t^2 \partial_z^2 w_2(x, z, t) + N_2^2 \partial_x^2 w_2(x, z, t) = 0, \quad z > H. \quad (\text{A1b})$$

Then, we consider a buoyancy source of the form $Q = B_0 \delta(t) \delta(x) \delta(z - z_0)$. Taking the Laplace transform in time ($t \rightarrow s$) and the Fourier transform in x ($x \rightarrow k$) of Eqs. (A1), we find

$$\partial_z^2 \hat{w}_1(x, z, t) + \lambda^2 \hat{w}_1(x, z, t) = \frac{\lambda^2}{\sqrt{2\pi} N_1^2} B_0 \delta(z - z_0), \quad z \leq H, \quad (\text{A2a})$$

$$\partial_z^2 \hat{w}_2(x, z, t) + \lambda_2^2 \hat{w}_2(x, z, t) = 0, \quad z > H, \quad (\text{A2b})$$

where $\lambda \equiv iN_1|k|/s$, and $\lambda_2 \equiv iN_2|k|/s$. The presence of $\delta(z - z_0)$ in the source term Q imposes a jump condition on w_1 at $z = z_0$, which we can find by integrating Eq. (A2a) twice in z :

$$[\hat{w}_1]_{-}^{+} = 0, \quad (\text{A3})$$

$$[\partial_z \hat{w}_1]_{-}^{+} = \frac{\lambda^2}{\sqrt{2\pi} N_1^2} B_0, \quad (\text{A4})$$

where $[]_{-}^{+}$ represents the difference across $z = z_0$.

We seek a solution subject to conditions at the surface ($z = 0$) and at the tropopause ($z = H$), as well as a radiation condition as $z \rightarrow \infty$. At the surface, the rigid lower boundary requires $\hat{w}_1 = 0$. At the tropopause ($z = H$), enforcing continuity of pressure and vertical

velocity requires $\hat{w}_1 = \hat{w}_2$ and $\partial_z \hat{w}_1 = \partial_z \hat{w}_2$. Above $z = H$, we require that $\hat{w}_2 \rightarrow 0$ as $z \rightarrow \infty$.

If the buoyancy frequency is constant (i.e., if $N = N_1$ everywhere), then the solution to the transformed Eqs. (A2) is

$$\hat{w}_1 = \hat{w}_2 \equiv \hat{w}_0^\pm = \begin{cases} -\frac{\lambda B_0}{\sqrt{2\pi}N_1^2} e^{i\lambda z_0} \sin(\lambda z), & 0 \leq z \leq z_0 \\ -\frac{\lambda B_0}{\sqrt{2\pi}N_1^2} \sin(\lambda z_0) e^{i\lambda z}, & z_0 < z \end{cases}. \quad (A5)$$

This solution applies throughout the whole atmosphere, so we have defined a new variable \hat{w}_0^\pm , where the plus sign refers to the solution for $z > z_0$ and minus sign refers to the solution for $z < z_0$.

Multiplying by $1/s$ in Laplace-transformed space is integration in time in real space, so we solve for the buoyancy by multiplying the \hat{w} solutions by $-N_1^2/s$ and inverting the Fourier and Laplace transforms. We find that the buoyancy due to a source term $Q = B_0 \delta(t) \delta(x) \delta(z - z_0)$ in an atmosphere with constant N is

$$b_{\text{point}}^{\text{no_lid}}(x, z, t) = \frac{B_0 N_1 t}{\pi x^2} \sin\left(\frac{N_1 t z}{x}\right) \sin\left(\frac{N_1 t z_0}{x}\right). \quad (A6)$$

To find the solution for the source term with baroclinic structure in the troposphere given by Eq. (8), we integrate Eq. (A6) against $\sin(mz_0)$ through the troposphere:

$$b_m^{\text{no_lid}}(x, z, t) = \int_0^H dz_0 \sin(mz_0) b_{\text{point}}^{\text{no_lid}}(x, z, t) \\ = \frac{B_0}{2\pi} \cos(mH) \sin(HN_1 t/x) \sin(N_1 t z/x) \\ \times \left(\frac{1}{N_1 t/m + x} + \frac{1}{N_1 t/m - x} \right), \quad (A7)$$

where m is one of the baroclinic modes. This is the Green's function for the constant- N atmosphere, which is Eq. (10) in the main text.

Now, suppose $N_2 = (1 + \gamma)N_1$, where $\gamma \geq -1$. While we cannot integrate the modified version of Eq. (A5) directly for the case $N_1 \neq N_2$, we can expand the modified version of Eq. (A5) in γ around $\gamma = 0$ and integrate each term in the series. By integrating enough terms and determining what the series converges to, we find a solution valid for all $\gamma \geq -1$ (i.e., for all $N_2 \geq 0$).

After rewriting \hat{w}_1 in terms of γ , we find

$$\hat{w}_1 = \begin{cases} -\frac{\lambda B_0}{\sqrt{2\pi}N_1^2} e^{i\lambda z_0} \sin(\lambda z) \left\{ \frac{1 + \frac{\gamma}{2} [1 - e^{2i\lambda(H-z_0)}]}{1 + \frac{\gamma}{2} (1 - e^{2i\lambda H})} \right\} & \text{for } 0 \leq z \leq z_0 \\ -\frac{\lambda B_0}{\sqrt{2\pi}N_1^2} \left(e^{i\lambda z_0} \sin(\lambda z) \left\{ \frac{1 + \frac{\gamma}{2} [1 - e^{2i\lambda(H-z_0)}]}{1 + \frac{\gamma}{2} (1 - e^{2i\lambda H})} \right\} - \sin[\lambda(z - z_0)] \right) & \text{for } z_0 < z \leq H \end{cases} \quad (A8)$$

and

$$\hat{w}_2 = -\frac{\lambda B_0}{\sqrt{2\pi}N_1^2} [e^{i\lambda z} \sin(\lambda z_0)] \left[\frac{e^{i\lambda \gamma(z-H)}}{1 + \frac{\gamma}{2} (1 - e^{2i\lambda H})} \right], \quad z > H. \quad (A9)$$

We focus our attention on the solution in the troposphere, Eq. (A8), which can be expanded about $\gamma = 0$ by noting that the denominator becomes

$$\left[1 + \frac{\gamma}{2} (1 - e^{2i\lambda H}) \right]^{-1} \approx 1 - \frac{\gamma}{2} (1 - e^{2i\lambda H}) \\ + \frac{\gamma^2}{4} (1 - e^{2i\lambda H})^2 - \dots. \quad (A10)$$

Recalling the constant- N solution \hat{w}_0^\pm , where the plus sign refers to the solution for $z > z_0$ and the minus sign refers to the solution for $z < z_0$, the first-order expansion in γ can be written as

$$\hat{w}_1 \approx \begin{cases} \hat{w}_0^- + \frac{\gamma}{2} e^{2i\lambda H} (1 - e^{-2i\lambda z_0}) \hat{w}_0^- & \text{for } 0 \leq z < z_0 \\ \hat{w}_0^+ + \frac{\gamma}{2} e^{2i\lambda H} (1 - e^{-2i\lambda z_0}) \hat{w}_0^- & \text{for } z_0 < z \leq H \end{cases}. \quad (A11)$$

Finding the higher-order terms is straightforward, and the n th-order term is

$$\left(\frac{\gamma}{2} \right)^n (e^{2i\lambda H} - 1)^{n-1} e^{2i\lambda H} (1 - e^{-2i\lambda z_0}) \hat{w}_0^-. \quad (A12)$$

As in the constant- N case, we solve for the buoyancy by multiplying by $-N_1^2/s$ and inverting the Laplace and Fourier transforms. In this way, we calculate

$$b_{\text{point}}^{\text{leaky}}(x, z, t) = b_{\text{point}}^{\text{no_lid}}(x, z, t) \times \frac{1 + \gamma}{1 + (2\gamma + \gamma^2) \sin^2\left(\frac{HN_1 t}{x}\right)} \quad \text{for } z \leq H. \quad (\text{A13})$$

The solution for $N_1 \neq N_2$ is just the constant- N solution (A6) multiplied by a new factor. Note that this expression does not rely on the smallness of γ ; it is valid over the entire range of N_2/N_1 from 0 to ∞ , which corresponds to $\gamma = -1$ to ∞ .

$$b_m^{\text{leaky}}(x, z, t) = b_m^{\text{no_lid}}(x, z, t) \times \frac{1 + \gamma}{1 + (2\gamma + \gamma^2) \sin^2\left(\frac{HN_1 t}{x}\right)} \quad \text{for } z \leq H. \quad (\text{A14})$$

This solution is the same as the tropospheric part of Eq. (13). Following a similar set of steps reveals the stratospheric part of the solution.

REFERENCES

- Battisti, D. S., E. S. Sarachik, and A. C. Hirst, 1999: A consistent model for the large-scale steady surface atmospheric circulation in the tropics. *J. Climate*, **12**, 2956–2964, doi:10.1175/1520-0442(1999)012<2956:ACMFTL>2.0.CO;2.
- Bretherton, C. S., and P. K. Smolarkiewicz, 1989: Gravity waves, compensating subsidence and detrainment around cumulus clouds. *J. Atmos. Sci.*, **46**, 740–759, doi:10.1175/1520-0469(1989)046<0740:GWCSAD>2.0.CO;2.
- Chan, I. H., and T. G. Shepherd, 2014: Diabatic balance model for the equatorial atmosphere. *J. Atmos. Sci.*, **71**, 985–1001, doi:10.1175/JAS-D-13-0224.1.
- Chang, C.-P., 1977: Viscous internal gravity waves and low-frequency oscillations in the tropics. *J. Atmos. Sci.*, **34**, 901–910, doi:10.1175/1520-0469(1977)034<0901:VIGWAL>2.0.CO;2.
- Chumakova, L. G., R. R. Rosales, and E. G. Tabak, 2013: Leaky rigid lid: New dissipative modes in the troposphere. *J. Atmos. Sci.*, **70**, 3119–3127, doi:10.1175/JAS-D-12-065.1.
- Cohen, B. G., and G. C. Craig, 2004: The response time of a convective cloud ensemble to a change in forcing. *Quart. J. Roy. Meteor. Soc.*, **130**, 933–944, doi:10.1256/qj.02.218.
- Edman, J. P., and D. M. Romps, 2014: An improved weak pressure gradient scheme for single-column modeling. *J. Atmos. Sci.*, **71**, 2415–2429, doi:10.1175/JAS-D-13-0327.1.
- Gill, A. E., 1980: Some simple solutions for heat-induced tropical circulation. *Quart. J. Roy. Meteor. Soc.*, **106**, 447–462, doi:10.1002/qj.49710644905.
- , 1982: *Atmosphere–Ocean Dynamics*. Academic Press, 662 pp.
- Haertel, P. T., and G. N. Kiladis, 2004: Dynamics of 2-day equatorial waves. *J. Atmos. Sci.*, **61**, 2707–2721, doi:10.1175/JAS3352.1.
- Hendon, H. H., and M. C. Wheeler, 2008: Some space–time spectral analyses of tropical convection and planetary-scale waves. *J. Atmos. Sci.*, **65**, 2936–2948, doi:10.1175/2008JAS2675.1.
- Lin, J.-L., B. E. Mapes, and W. Han, 2008: What are the sources of mechanical damping in Matsuno–Gill-type models? *J. Climate*, **21**, 165–179, doi:10.1175/2007JCLI1546.1.
- Lin, Y. L., and R. B. Smith, 1986: Transient dynamics of airflow near a local heat source. *J. Atmos. Sci.*, **43**, 40–49, doi:10.1175/1520-0469(1986)043<0040:TDOANA>2.0.CO;2.
- Lindzen, R. S., 2003: The interaction of waves and convection in the tropics. *J. Atmos. Sci.*, **60**, 3009–3020, doi:10.1175/1520-0469(2003)060<3009:TIOAWC>2.0.CO;2.
- Mapes, B. E., 1993: Gregarious tropical convection. *J. Atmos. Sci.*, **50**, 2026–2037, doi:10.1175/1520-0469(1993)050<2026:GTC>2.0.CO;2.
- , 1998: The large-scale part of tropical mesoscale convective system circulations: A linear vertical spectral band model. *J. Meteor. Soc. Japan*, **76**, 29–55, doi:10.2151/jmsj1965.76.1_29.
- , 2000: Convective inhibition, subgrid-scale triggering energy, and stratiform instability in a toy tropical wave model. *J. Atmos. Sci.*, **57**, 1515–1535, doi:10.1175/1520-0469(2000)057<1515:CISSTE>2.0.CO;2.
- , and R. A. Houze, 1995: Diabatic divergence profiles in western Pacific mesoscale convective systems. *J. Atmos. Sci.*, **52**, 1807–1828, doi:10.1175/1520-0469(1995)052<1807:DDPIWP>2.0.CO;2.
- Matsuno, T., 1966: Quasi-geostrophic motions in the equatorial area. *J. Meteor. Soc. Japan*, **44**, 25–43, doi:10.2151/jmsj1965.44.1_25.
- Neelin, J., and I. Held, 1987: Modeling tropical convergence based on the moist static energy budget. *Mon. Wea. Rev.*, **115**, 3–12, doi:10.1175/1520-0493(1987)115<0003:MTCBOT>2.0.CO;2.
- Pandya, R., D. R. Durran, and C. Bretherton, 1993: Comments on “Thermally forced gravity waves in an atmosphere at rest.” *J. Atmos. Sci.*, **50**, 4097–4101, doi:10.1175/1520-0469(1993)050<4097:COFGWI>2.0.CO;2.
- Raymond, D., and X. Zeng, 2000: Instability and large-scale circulations in a two-column model of the tropical troposphere. *Quart. J. Roy. Meteor. Soc.*, **126**, 3117–3135, doi:10.1002/qj.49712657007.
- Romps, D. M., 2014: Rayleigh damping in the free troposphere. *J. Atmos. Sci.*, **71**, 553–565, doi:10.1175/JAS-D-13-062.1.

- Sobel, A., J. Nilsson, and L. Polvani, 2001: The weak temperature gradient approximation and balanced tropical moisture waves. *J. Atmos. Sci.*, **58**, 3650–3665, doi:[10.1175/1520-0469\(2001\)058<3650:TWTGAA>2.0.CO;2](https://doi.org/10.1175/1520-0469(2001)058<3650:TWTGAA>2.0.CO;2).
- Sugiyama, M., 2009: The moisture mode in the quasi-equilibrium tropical circulation model. Part I: Analysis based on the weak temperature gradient approximation. *J. Atmos. Sci.*, **66**, 1507–1523, doi:[10.1175/2008JAS2690.1](https://doi.org/10.1175/2008JAS2690.1).
- Wheeler, M., and G. N. Kiladis, 1999: Convectively coupled equatorial waves: Analysis of clouds and temperature in the wavenumber frequency domain. *J. Atmos. Sci.*, **56**, 374–399, doi:[10.1175/1520-0469\(1999\)056<0374:CCEWAO>2.0.CO;2](https://doi.org/10.1175/1520-0469(1999)056<0374:CCEWAO>2.0.CO;2).
- Wu, Z., E. Sarachik, and D. Battisti, 2000: Vertical structure of convective heating and the three-dimensional structure of the forced circulation on an equatorial beta plane. *J. Atmos. Sci.*, **57**, 2169–2187, doi:[10.1175/1520-0469\(2000\)057<2169:VSOCHA>2.0.CO;2](https://doi.org/10.1175/1520-0469(2000)057<2169:VSOCHA>2.0.CO;2).
- Yano, J., and K. Emanuel, 1991: An improved model of the equatorial troposphere and its coupling with the stratosphere. *J. Atmos. Sci.*, **48**, 377–389, doi:[10.1175/1520-0469\(1991\)048<0377:AIMOTE>2.0.CO;2](https://doi.org/10.1175/1520-0469(1991)048<0377:AIMOTE>2.0.CO;2).